Evolution of Wrinkles in Elastic-Viscoelastic Bilayer Thin Films

S. H. Im

R. Huang
e-mail: ruihuang@mail.utexas.edu

Center for Mechanics of Solids, Structures and Materials,
Department of Aerospace Engineering and Engineering Mechanics,
The University of Texas,
Austin, TX 78712

This paper develops a model for evolving wrinkles in a bilayer thin film consisting of an elastic layer and a viscoelastic layer. The elastic layer is subjected to a compressive residual stress and is modeled by the nonlinear von Karman plate theory. A thin-layer approximation is developed for the viscoelastic layer. The stability of the bilayer and the evolution of wrinkles are studied first by a linear perturbation analysis and then by numerical simulations. Three stages of the wrinkle evolution are identified: initial growth of the fastest growing mode, intermediate growth with mode transition, and, finally, an equilibrium wrinkle state. [DOI: 10.1115/1.2043191]

1 Introduction

Complex wrinkle patterns have been observed in various thin-film systems, typically with integrated hard and soft materials. The wrinkles are a nuisance in some applications [1,2], but may be used as stretchable interconnects for flexible electronics [3,4] or biological assays [5]. Diverse wrinkle patterns can be generated by engineering the surface structures or chemistry with potential applications for micro- and nanoscale fabrication [6,7]. It is also possible to extract mechanical properties (e.g., elastic modulus and residual stress) of both organic and inorganic thin-film materials from wrinkle patterns [8,9]. Quantitative understanding of the wrinkling behavior is essential for these applications.

The underlying mechanism of wrinkling has been generally understood as a stress-driven instability, similar to Euler buckling of an elastic column under compression. For a solid film bonded to a substrate, however, the instability is constrained. If the substrate is elastic, there exists a critical compressive stress beyond which the film wrinkles with a particular wavelength selected by minimizing the total elastic energy in the film and the substrate [10–12]. Under a typical compressive stress, a wrinkle forms when the substrate is considerably softer than the film. If the substrate is viscous (e.g., glasses and polymers at high temperatures), wrinkling becomes a kinetic process [13,14]. Since the viscous substrate does not store elastic energy, a compressed blanket film on top is always energetically unstable. The viscous flow in the substrate controls the kinetics of wrinkle growth, selecting a fastest growing wavelength. More generally, if the substrate is viscoelastic (e.g., cross-linked polymers), both energetics and kinetics play important roles. A spectrum of evolving wrinkle patterns has been observed, experimentally, in metal/polymer bilayers [15], exhibiting a peculiar kinetic process. A linear perturbation analysis has shown that the viscoelastic property of the substrate has a profound effect on the stability and kinetics of the wrinkling process [16]. This paper develops a model that allows direct simulation of wrinkle evolution in thin elastic-viscoelastic bilayers beyond the limit of linear perturbation analysis.

The plan of the paper is as follows. Section 2 presents the model formulation, which consists of a summary of the nonlinear von Karman plate theory for the elastic layer and the development of a thin-layer approximation for the viscoelastic layer. Although the model is applicable for two-dimensional wrinkle patterns, the remainder of this study focuses on one-dimensional wrinkles under the plane-strain condition. Section 3 performs a linear perturbation analysis. Section 4 reviews a solution for the equilibrium state at the elastic limit. In Sec. 5, numerical simulations are conducted, showing the transient evolution process. Section 6 concludes with a summary of results.

2 Model Formulation

Figure 1 shows the model structure considered in this study: an elastic layer of thickness h_f lying on a viscoelastic layer of thickness H, which, in turn, lies on a rigid substrate. At the reference state (Fig. 1(a)), both layers are flat, and the elastic layer is subjected to an in-plane biaxial compressive stress σ_0 (i.e., $\sigma_0<0$). The surface of the bilayer is free of tractions. Upon wrinkling (Fig. 1(b)), the elastic layer undergoes both in-plane and out-of-plane displacements to relax the residual stress, and the viscoelastic layer deforms concomitantly. Both the upper and lower interfaces of the viscoelastic layer are assumed to remain bonded. This section develops a model that couples the elastic and viscoelastic deformation in the bilayer. For convenience, a Cartesian coordinate system is set up with the x_1-x_2 plane coinciding with the interface between the two layers, as shown in Fig. 1(a).

2.1 Deformation of the Elastic Layer. We employ the nonlinear von Karman plate theory [17] to model the elastic layer. Let w be the lateral deflection, u_α the in-plane displacement ($\alpha=1,2$), q the normal traction at the interface with the viscoelastic layer, and τ_α the shear tractions at the same interface. Equilibrium requires that

$$q=-D_f\frac{\partial^4 w}{\partial x_\alpha \partial x_\alpha \partial x_\beta \partial x_\beta}+N_{\alpha\beta}\frac{\partial^2 w}{\partial x_\alpha \partial x_\beta}+\tau_\alpha\frac{\partial w}{\partial x_\alpha} \tag{1}$$

$$\tau_\alpha=\frac{\partial N_{\alpha\beta}}{\partial x_\beta} \tag{2}$$

where

$$D_f=\frac{E_f h_f^3}{12(1-\nu_f^2)} \tag{3}$$

$$N_{\alpha\beta}=\sigma_0 h_f \delta_{\alpha\beta}+\frac{E_f h_f}{1-\nu_f^2}[(1-\nu_f)\varepsilon_{\alpha\beta}+\nu_f \varepsilon_{\gamma\gamma}\delta_{\alpha\beta}] \tag{4}$$

Contributed by the Applied Mechanics Division of The American Society of Mechanical Engineers for publication in the ASME Journal of Applied Mechanics. Manuscript received by the Applied Mechanics Division, May 23, 2003; final revision; March 24, 2005. Associate Editor: A. A. Ferri. Discussion on the paper should be addressed to the Editor, Prof. Robert M. McMeeking, Journal of Applied Mechanics, Department of Mechanical and Environmental Engineering, University of California—Santa Barbara, Santa Barbara, CA 93106-5070, and will be accepted until four months after final publication in the paper itself in the ASME Journal of Applied Mechanics.

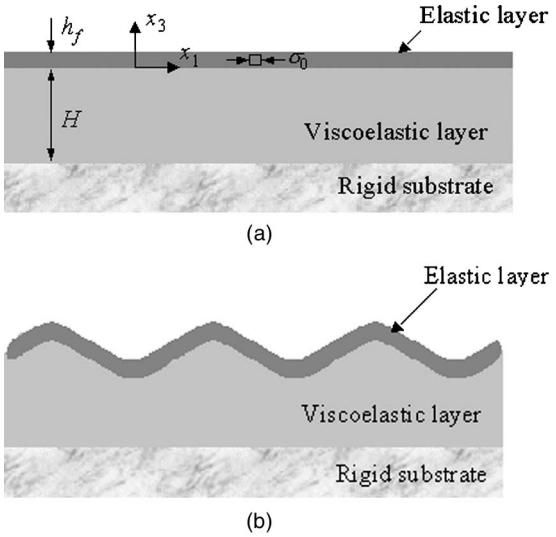

Fig. 1 Schematic of an elastic-viscoelastic bilayer on a rigid substrate: (*a*) the reference state and (*b*) a wrinkled state

$$\varepsilon_{\alpha\beta}=\frac{1}{2}\left(\frac{\partial u_\alpha}{\partial x_\beta}+\frac{\partial u_\beta}{\partial x_\alpha}\right)+\frac{1}{2}\frac{\partial w}{\partial x_\alpha}\frac{\partial w}{\partial x_\beta} \tag{5}$$

Here E_f is the Young's modulus of the elastic layer, ν_f the Poisson's ratio, D_f the flexural rigidity, $N_{\alpha\beta}$ the in-plane membrane force, $\varepsilon_{\alpha\beta}$ the in-plane strain, and $\delta_{\alpha\beta}$ the Kronecker delta. The Greek subscripts α and β take on the values of the in-plane coordinates 1 and 2, and a repeated Greek subscript implies summation over 1 and 2.

Note that, a nonlinear term is included in Eq. (5) to account for moderately large deflections of the elastic layer. In addition, the coupling between the in-plane deformation and the lateral deflection in Eq. (1) introduces further nonlinearity. The nonlinear equations have been widely used for analyses of buckle-delamination in thin films [18].

2.2 Deformation of a Viscoelastic Thin-Layer. Next consider the viscoelastic layer. The linear theory of viscoelasticity [19] is adopted, where the stress-strain relation is described in an integral form with a shear relaxation modulus $\mu(t)$ and Poisson's ratio $\nu(t)$, both time dependent, in general. The Laplace transform of the stress-strain relation has a form identical to that of linear elasticity with the elastic shear modulus μ and Poisson's ratio ν replaced by $s\bar{\mu}(s)$ and $s\bar{\nu}(s)$, respectively, where a bar over a variable designates its Laplace transform with respect to time t and s is the transform variable. Therefore, the Laplace transformed solution of a viscoelastic problem can be obtained directly from the solution of a corresponding elastic problem, namely, the correspondence principle. The final solution for the viscoelastic problem can then be realized upon inverting the transformed solution.

For the present study, the viscoelastic layer is stress free initially ($t=0$) and subjected to normal and shear tractions at the top surface for $t>0$, namely,

$$\sigma_{33}=S_3(x_1,x_2,t) \quad \text{and} \quad \sigma_{3\alpha}=S_\alpha(x_1,x_2,t) \text{ at } x_3=0 \tag{6}$$

At the lower interface, the displacement is fixed

$$u_\alpha=u_3=0 \text{ at } x_3=-H \tag{7}$$

In the following, a thin-layer approximation is developed to solve for the response of the viscoelastic layer subjected to arbitrary tractions.

A previous study by Huang [16] solved a similar problem, but under the plane-strain condition, where $S_2=u_2=0$, and the tractions at the top surface take the form

$$S_1=A(t)\sin kx_1 \tag{8}$$

$$S_3=B(t)\cos kx_1 \tag{9}$$

with a constant wave number k and arbitrarily time-dependent amplitudes $A(t)$ and $B(t)$. The Laplace transform of the displacements at the top surface was obtained as follows:

$$\bar{u}_1(x_1,s)=\frac{1}{2ks\bar{\mu}(s)}[\gamma_{11}(s\bar{\nu},kH)\bar{A}(s)+\gamma_{12}(s\bar{\nu},kH)\bar{B}(s)]\sin(kx_1) \tag{10}$$

$$\bar{u}_3(x_1,s)=\frac{1}{2ks\bar{\mu}(s)}[\gamma_{21}(s\bar{\nu},kH)\bar{A}(s)+\gamma_{22}(s\bar{\nu},kH)\bar{B}(s)]\cos(kx_1) \tag{11}$$

where

$$\gamma_{11}=\frac{1+\kappa}{4}\frac{\kappa\sinh(2kH)+2kH}{\kappa\cosh^2(kH)+(kH)^2+\left(\frac{1-\kappa}{2}\right)^2} \tag{12}$$

$$\gamma_{22}=\frac{1+\kappa}{4}\frac{\kappa\sinh(2kH)-2kH}{\kappa\cosh^2(kH)+(kH)^2+\left(\frac{1-\kappa}{2}\right)^2} \tag{13}$$

$$\gamma_{12}=\gamma_{21}=-\frac{\frac{\kappa(1-\kappa)}{2}\sinh^2(kH)+(kH)^2}{\kappa\cosh^2(kH)+(kH)^2+\left(\frac{1-\kappa}{2}\right)^2} \tag{14}$$

and $\kappa=3-4s\bar{\nu}(s)$.

The above solution shows that, in general, the surface of the viscoelastic layer undergoes both out-of-plane and in-plane displacements and they are coupled. However, in two special cases, the two displacements can be decoupled. In the first case, the viscoelastic layer is infinitely thick ($kH\to\infty$) and incompressible ($\nu=0.5$), which has been considered in the previous study [16]. In the other case, as will be considered in the present study, the viscoelastic layer is very thin ($kH\to 0$), for which Eqs. (10) and (11) reduce to

$$\bar{u}_1(x_1,s)=\frac{1}{2ks\bar{\mu}(s)}\left[2kH\bar{A}(s)-\frac{1-4\nu}{2(1-\nu)}(kH)^2\bar{B}(s)\right]\sin(kx_1) \tag{15}$$

$$\bar{u}_3(x_1,s)=\frac{1}{2ks\bar{\mu}(s)}\left[\frac{1-2\nu}{1-\nu}(kH)\bar{B}(s)-\frac{1-4\nu}{2(1-\nu)}(kH)^2\bar{A}(s)\right]\cos(kx_1) \tag{16}$$

By the thin-layer approximation, only the leading terms in kH are retained in Eqs. (15) and (16). In addition, the Poisson's ratio has been assumed to be a constant independent of time, considering the factor that the Poisson's ratio is typically a weak function of time. If the viscoelastic layer is incompressible (i.e., $\nu=0.5$), however, Eq. (16) takes a different form

$$\bar{u}_3(x_1,s)=\frac{1}{2ks\bar{\mu}(s)}\left[\frac{2}{3}(kH)^3\bar{B}(s)+(kH)^2\bar{A}(s)\right]\cos(kx_1) \tag{17}$$

where the first term in the brackets scales with $(kH)^3$ instead of kH in Eq. (16). On the other hand, Eq. (15) remains valid. As will be shown later, this leads to different kinetics of wrinkling for compressible and incompressible viscoelastic layers.

To be specific, consider the Kelvin model of linear viscoelas-

ticity, modeled by a mechanical analog consisting of a spring and a dashpot in parallel, for which the relaxation modulus is

$$\mu(t) = \mu_\infty + \eta\delta(t) \tag{18}$$

where μ_∞ is the stiffness of the spring, representing the elastic shear modulus at the rubbery limit, and η is the viscosity. The Laplace transform of the relaxation modulus is

$$\bar{\mu}(s) = \frac{\mu_\infty}{s} + \eta \tag{19}$$

After substituting (19) into Eqs. (15) and (16), inverse Laplace transform leads to

$$\frac{\partial u_1}{\partial t} = \frac{H}{\eta}S_1 - \frac{1-4\nu}{4(1-\nu)}\frac{H^2}{\eta}\frac{\partial S_3}{\partial x_1} - \frac{\mu_\infty}{\eta}u_1 \tag{20}$$

$$\frac{\partial u_3}{\partial t} = \frac{1-2\nu}{2(1-\nu)}\frac{H}{\eta}S_3 + \frac{1-4\nu}{4(1-\nu)}\frac{H^2}{\eta}\frac{\partial S_1}{\partial x_1} - \frac{\mu_\infty}{\eta}u_3 \tag{21}$$

Similarly, for an incompressible viscoelastic layer (ν=0.5), the inverse transform of Eq. (17) leads to

$$\frac{\partial u_3}{\partial t} = -\frac{H^3}{3\eta}\frac{\partial^2 S_3}{\partial x_1^2} - \frac{H^2}{2\eta}\frac{\partial S_1}{\partial x_1} - \frac{\mu_\infty}{\eta}u_3 \tag{22}$$

Equations (20) and (22) have the similar form as the Reynold's lubrication theory for nearly parallel flow of a thin liquid layer [14,20], but with an additional term accounting for the elastic limit of the viscoelastic layer.

For the present study, we assume a compressible viscoelastic layer (i.e., $\nu \neq 0.5$) and further neglect the H^2 terms in Eqs. (20) and (21) for thin-layer approximation, which leads to

$$\frac{\partial u_1}{\partial t} = \frac{H}{\eta}S_1 - \frac{\mu_\infty}{\eta}u_1, \tag{23}$$

$$\frac{\partial u_3}{\partial t} = \frac{1-2\nu}{2(1-\nu)}\frac{H}{\eta}S_3 - \frac{\mu_\infty}{\eta}u_3 \tag{24}$$

Here the two traction components are assumed to have comparable magnitudes and the thickness of the viscoelastic layer is assumed to be small compared to the wavelength ($L=2\pi/k$). Equation (23) is equivalent to a shear lag model, which assumes uniform shear stress across the thin layer. Similar models have been used for both elastic and viscous layers [21,22]. Equation (24) is similar to the Winkler model for elastic foundation [23] but includes a time derivative term due to the viscous effect. The two equations are uncoupled under the thin-layer approximation.

In the above development, plane-strain deformation and periodic surface tractions have been assumed. The restriction of periodic tractions has been relaxed by using differentiation of the surface tractions with respect to x_1 in places of the particular wave number after inverse Laplace transform. The resulting equations, (20) and (21), are apparently independent of wave number and can be used for arbitrary tractions by linear superposition of their Fourier components. At the end, the in-plane and out-of-plane responses are decoupled by the thin-layer approximation. Therefore, the restriction of plane-strain deformation can be relaxed by generalizing the in-plane response, Eq. (23), for both x_1 and x_2 directions, which leads to

$$\frac{\partial u_\alpha}{\partial t} = \frac{H}{\eta}S_\alpha - \frac{\mu_\infty}{\eta}u_\alpha \tag{25}$$

for α=1,2. Equations (24) and (25) then represent the approximate solution for the three-dimensional response of a thin viscoelastic layer subjected to the boundary conditions in Eqs. (6) and (7).

In the case of an incompressible viscoelastic layer, however, the Winkler-type equation for the out-of-plane displacement (Eq. (24)) breaks down and the decoupling is not applicable. The coupled equations, (20) and (22), must be used in this case. Generalization of the plane-strain response to the three-dimensional would take the similar form as the lubrication theory [14], but will not be further pursued in the present study.

2.3 Coupled Evolution Equations. The interface between the elastic and viscoelastic layers is assumed to remain bonded during deformation. Consequently, the displacements and tractions are continuous across the interface, which couples the equilibrium equations of the elastic layer, Eqs. (1) and (2), with the time-dependent responses of the viscoelastic layer, Eqs. (24) and (25), and leads to

$$\frac{\partial w}{\partial t} = \frac{1-2\nu}{2(1-\nu)}\frac{H}{\eta}\left(-D_f\frac{\partial^4 w}{\partial x_\alpha \partial x_\alpha \partial x_\beta \partial x_\beta} + N_{\alpha\beta}\frac{\partial^2 w}{\partial x_\alpha \partial x_\beta} + \frac{\partial N_{\alpha\beta}}{\partial x_\beta}\frac{\partial w}{\partial x_\alpha}\right) - \frac{\mu_\infty}{\eta}w \tag{26}$$

$$\frac{\partial u_\alpha}{\partial t} = \frac{H}{\eta}\frac{\partial N_{\alpha\beta}}{\partial x_\beta} - \frac{\mu_\infty}{\eta}u_\alpha \tag{27}$$

Equations (26) and (27) are coupled, nonlinear evolution equations, which may be solved numerically to simulate three-dimensional deformation of an elastic-viscoelastic bilayer and evolution of the resulting two-dimensional wrinkle patterns. In the remainder of this paper, however, we focus our attention on plane-strain deformation and one-dimensional wrinkles only, leaving the two-dimensional wrinkles for a subsequent study. The reduced equations for the plane-strain wrinkles are summarized as follows:

$$\frac{\partial w}{\partial t} = \frac{1-2\nu}{2(1-\nu)}\frac{H}{\eta}\left(-D_f\frac{\partial^4 w}{\partial x^4} + N\frac{\partial^2 w}{\partial x^2} + \frac{\partial N}{\partial x}\frac{\partial w}{\partial x}\right) - \frac{\mu_\infty}{\eta}w \tag{28}$$

$$\frac{\partial u}{\partial t} = \frac{H}{\eta}\frac{\partial N}{\partial x} - \frac{\mu_\infty}{\eta}u \tag{29}$$

$$N = \sigma_0 h_f + \frac{E_f h_f}{1-\nu_f^2}\left[\frac{\partial u}{\partial x} + \frac{1}{2}\left(\frac{\partial w}{\partial x}\right)^2\right] \tag{30}$$

Recently, Huang et al. [24] developed a similar model to simulate the evolution of two-dimensional wrinkle patterns in elastic films on soft substrates, where the viscoelastic Kelvin model was used to relate the lateral deflection and the normal traction, similar to Eq. (24), but the relation between the in-plane displacement and the shear traction was taken to be linear elastic. While the attention there was focused on various equilibrium wrinkle patterns, the interest of the present study is the temporal evolution of wrinkles.

3 Linear Perturbation Analysis

Assume a small deflection of the elastic layer in the form of

$$w(x,t) = A(t)\cos kx \tag{31}$$

For the linear perturbation analysis, the evolution of the in-plane displacement is uncoupled from the lateral deflection and, therefore, ignored. Inserting (31) into Eq. (28) and retaining only the leading-order terms in A, we obtain that

$$\frac{dA}{dt} = \frac{\alpha E_f - \mu_\infty}{\eta}A(t) \tag{32}$$

where

$$\alpha = \frac{(1-2\nu)k^2 H h_f}{24(1-\nu)(1-\nu_f^2)}\left[-k^2 h_f^2 - \frac{12(1-\nu_f^2)\sigma_0}{E_f}\right] \tag{33}$$

Solving Eq. (32) leads to

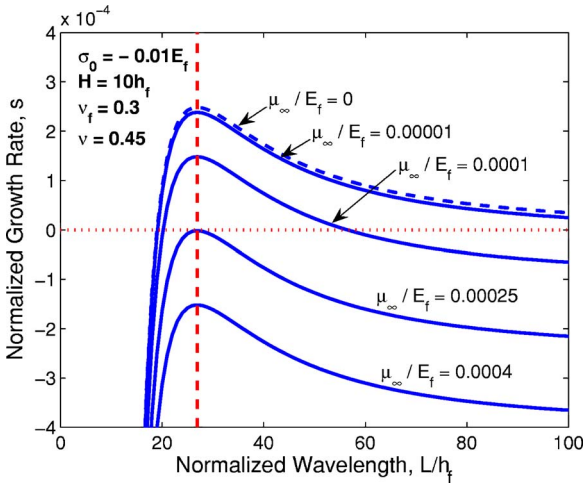

Fig. 2 Initial growth rate as a function of wavelength by the linear perturbation analysis, for various ratios between the rubbery modulus of the viscoelastic layer and the Young's modulus of the elastic layer

$$A(t) = A_0 \exp\left(s\frac{t}{\tau}\right) \tag{34}$$

where A_0 is the initial perturbation amplitude, $\tau = \eta/E_f$ is a characteristic time scale, and $s = \alpha - \mu_\infty/E_f$ is the dimensionless growth rate of the perturbation. The stability of the bilayer therefore depends on the sign of the growth rate. If $s<0$ for all wave numbers k, the bilayer is stable and remains flat. Otherwise, if $s>0$ for any permissible wave numbers, the bilayer is unstable and perturbations grow to form wrinkles. In this case, the amplitude grows exponentially with time at the initial stage. A more sophisticated analysis [16] has shown that the initial growth can be nonexponential if the viscoelastic layer has a finite elastic modulus at the glassy state (elastic limit as $t \to 0$).

Figure 2 plots the growth rate as a function of the perturbation wavelength ($L=2\pi/k$) for different ratios between the rubbery modulus of the viscoelastic layer and the elastic modulus of the elastic layer. At the limiting case when $\mu_\infty=0$, $s=\alpha$ and the growth rate is positive (recall that $\sigma_0<0$) for long wave perturbations, as shown by the dashed line in Fig. 2. Consequently, the bilayer is always unstable. The critical wavelength is

$$L_c = \pi h_f \sqrt{-\frac{E_f}{3(1-\nu_f^2)\sigma_0}} \tag{35}$$

which is identical to the critical length of Euler buckling. The growth rate is positive when $L>L_c$ and peaks at the wavelength

$$L_m = \pi h_f \sqrt{-\frac{2E_f}{3(1-\nu_f^2)\sigma_0}} \tag{36}$$

Similar results were obtained for an elastic film on a viscous layer [14,25], where the fastest growing wavelength L_m is, however, shorter by 13.4% due to the incompressibility of the viscous layer. Using typical values for a thin aluminum layer: $E_f=70$ GPa, $\nu_f=0.35$, $h_f=40$ nm, and $\sigma_0=-100$ MPa, we obtain $L_c=2.05$ μm and $L_m=2.90$ μm. The latter compares closely to the initial wavelengths observed in experiments by Yoo and Lee [15] despite the rough estimate of the stress.

As the ratio μ_∞/E_f increases, the growth rate decreases; the curve in Fig. 2 shifts down, but without any change in the shape. As a result, the critical wavelength increases, and a second critical wavelength emerges at the long wave end. The growth rate is now positive within a window bounded by the two critical wavelengths. On the other hand, the fastest growing wavelength does not change, but the corresponding growth rate decreases. The fastest growth rate reduces to zero at a critical ratio

$$\left(\frac{\mu_\infty}{E_f}\right)_c = \frac{3(1-\nu_f^2)(1-2\nu)}{2(1-\nu)}\frac{H}{h_f}\left(\frac{\sigma_0}{E_f}\right)^2 \tag{37}$$

The bilayer becomes stable when μ_∞/E_f is greater than the critical ratio. Alternatively, Eq. (37) may be rewritten to give the critical compressive stress, below which a bilayer with the given thickness ratio and moduli ratio is stable. The critical condition is identical to that for an elastic film on a thin elastic substrate with the shear modulus $\mu=\mu_\infty$ [12,16].

It is noted that, by the critical condition in Eq. (37), the stability of an elastic-viscoelastic bilayer depends on the rubbery modulus (i.e., the long-term limit of the relaxation modulus) of the viscoelastic layer, but independent of the initial modulus (e.g., the glassy state). In other words, despite that the viscoelastic layer is initially stiff or even rigid, the bilayer "foresees" the subsequent softening of the layer and becomes unstable spontaneously. The time scale of wrinkle growth is proportional to the viscosity, and the growth rate increases as the rubbery modulus decreases. The wavelength of the fastest growing mode, however, is independent of the viscoelastic layer, as given in Eq. (36). Our previous study [16] showed that the fastest growing wavelength weakly depends on the thickness ratio and Poisson's ratio. The thin-layer approximation in the present study leads to a reasonably accurate wavelength, but underestimates the growth rate for the fastest growing mode when the thickness ratio H/h_f is larger than 2.

4 Equilibrium Wrinkles

Setting $\partial/\partial t=0$ in Eqs. (28) and (29) leads to two coupled nonlinear ordinary differential equations, from which one can solve for equilibrium states. The solution is identical to that for an elastic film on a thin elastic substrate with the shear modulus $\mu=\mu_\infty$. The latter has been obtained by an energy minimization procedure [12,16], as summarized below. First, the equilibrium amplitude of a sinusoidal wrinkle with a wave number k is given by

$$A_{eq} = \frac{2\sqrt{1-\nu_f^2}}{k}\left[-\frac{\sigma_0}{E_f} - \frac{(kh_f)^2}{12(1-\nu_f^2)} - \frac{2(1-\nu)}{1-2\nu}\frac{\mu_\infty}{E_f}\frac{1}{k^2 H h_f}\right]^{1/2} \tag{38}$$

It can be confirmed that only when the bilayer is unstable does there exist nonzero, real-valued equilibrium wrinkle amplitudes. Furthermore, minimization of the elastic strain energy in the bilayer with respect to the wave number selects an equilibrium wrinkle wavelength

$$L_{eq} = \pi h_f \left[\frac{2(1-2\nu)}{3(1-\nu)(1-\nu_f^2)}\frac{E_f}{\mu_\infty}\frac{H}{h_f}\right]^{1/4} \tag{39}$$

The corresponding wrinkle amplitude can be obtained from Eq. (38) with $k=2\pi/L_{eq}$. Again, using typical values: $E_f=70$ GPa, $\nu_f=0.35$, $h_f=40$ nm, $\mu_\infty=0.01$ MPa, $\nu=0.45$, $H=400$ nm, and $\sigma_0=-100$ MPa, we obtain $L_{eq}=7.00$ μm and $A_{eq}=71.9$ nm. It is noted that Eq. (39) underestimates the equilibrium wavelength when the thickness ratio H/h_f is larger than 2.

Comparing the equilibrium wrinkle wavelength to the initially fastest growing wavelength given by Eq. (36), we note that the two wavelengths can be totally independent. The fastest growing wavelength, which dominates the initial growth, is determined by the kinetics and depends on the compressive stress in the elastic layer, but independent of the viscoelastic layer. The equilibrium wavelength, on the other hand, is determined by energetics and depends on the thickness and rubbery modulus of the viscoelastic layer, but independent of the stress in the elastic layer. Such independence may enable simultaneous determination of the residual stress and rubbery modulus from the initial and final wrinkle wavelengths, respectively.

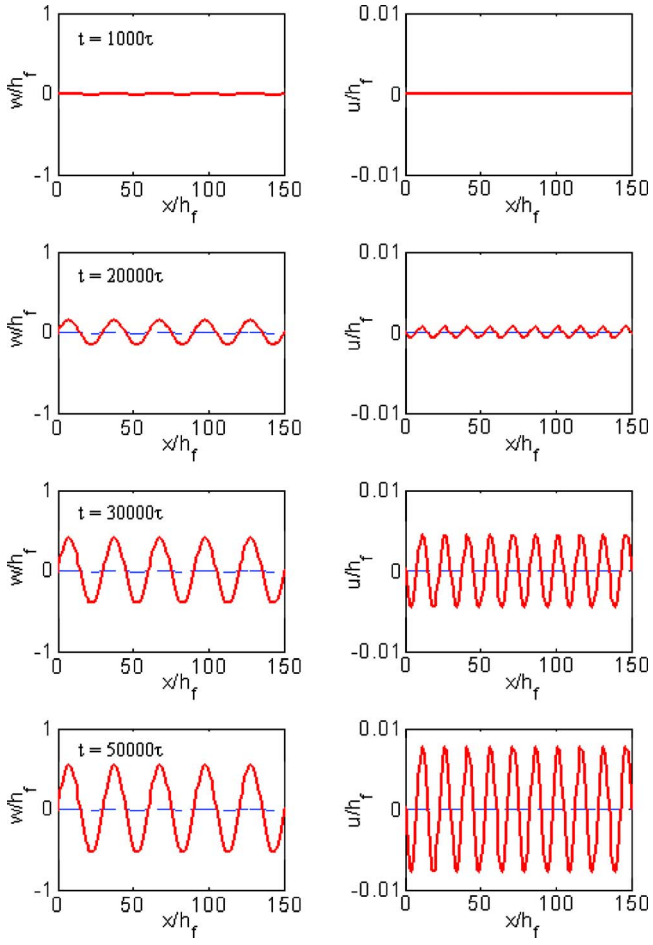

Fig. 3 Evolution of the lateral deflection *w* and the in-plane displacement *u* by numerical simulation with a sinusoidal initial perturbation

At the equilibrium state, the shear traction at the interface is nearly zero and the lateral displacement approximately takes the form [12,14]

$$u = \tfrac{1}{8} k A_{eq}^2 \sin(2kx) \tag{40}$$

where $k = 2\pi / L_{eq}$. The wavelength of the in-plane displacement is half of the wrinkle wavelength at the equilibrium state.

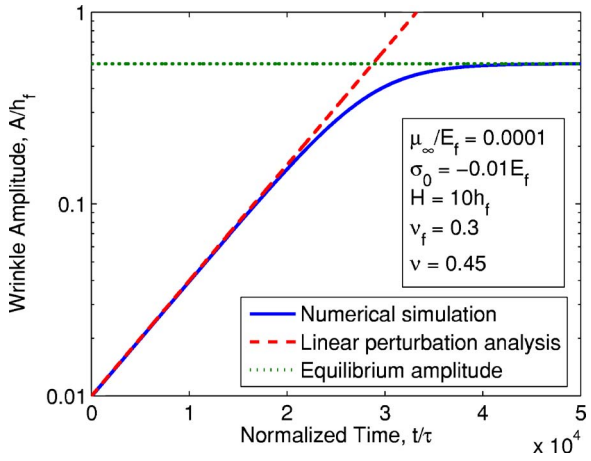

Fig. 4 Amplitude of a sinusoidal wrinkle as a function of time

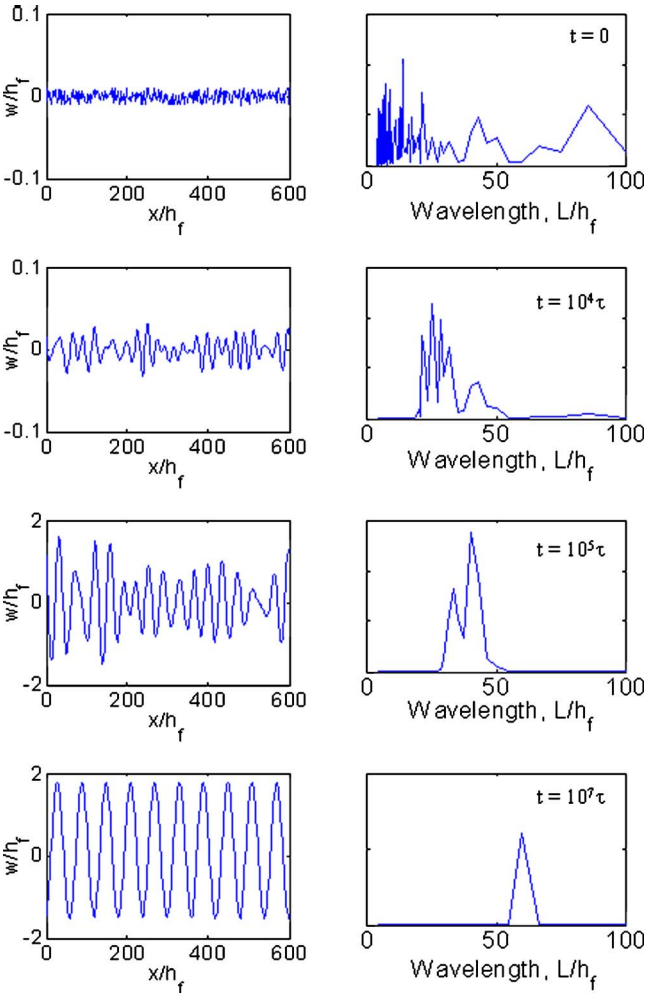

Fig. 5 Numerical simulation of evolving wrinkles with a random initial perturbation. The left column shows the deflection of the elastic layer, and the right column shows the corresponding Fourier spectra.

5 Numerical Simulations

In this section, we simulate the evolution of wrinkles by numerically integrating the nonlinear equations, (28) and (29). For simplicity, we use the explicit forward-time-center-space (FTCS) finite difference method. The algorithm is conditionally stable. To achieve sufficient accuracy, a small space step Δx is first specified. Next, the time step Δt is determined by the stability and convergence of the numerical results. In the following simulations, we use $\Delta x = 1.0 h_f$ and $\Delta t = 0.1 \eta / E_f$. The time is normalized by the time scale $\tau = \eta / E_f$, which ranges widely from 1 μs to 1 s, depending on the material of the viscoelastic layer and the temperature. In all simulations, the periodic boundary condition is assumed.

The bilayer is in equilibrium at the reference state (Fig. 1(*a*)) with no tractions at the interface. By introducing a small perturbation displacement to the reference state as the initial condition, the system evolves until it reaches another equilibrium state. First, we start with a sinusoidal deflection of amplitude $A_0 = 0.01 h_f$ and zero in-plane displacement at $t = 0$. The wavelength $L = 30 h_f$ was selected to be close to the fastest growing wavelength ($L_m = 26.9 h_f$) to save the computational time. Other parameters are $\sigma_0 = -0.01 E_f$, $\mu_\infty = 0.0001 E_f$, $H = 10 h_f$, $\nu_f = 0.3$, and $\nu = 0.45$. As noted before, the present model underestimates the growth rate and the equilibrium wavelength for thick viscoelastic layers ($H > 2 h_f$). Nevertheless, the wrinkling kinetics should be similar, and

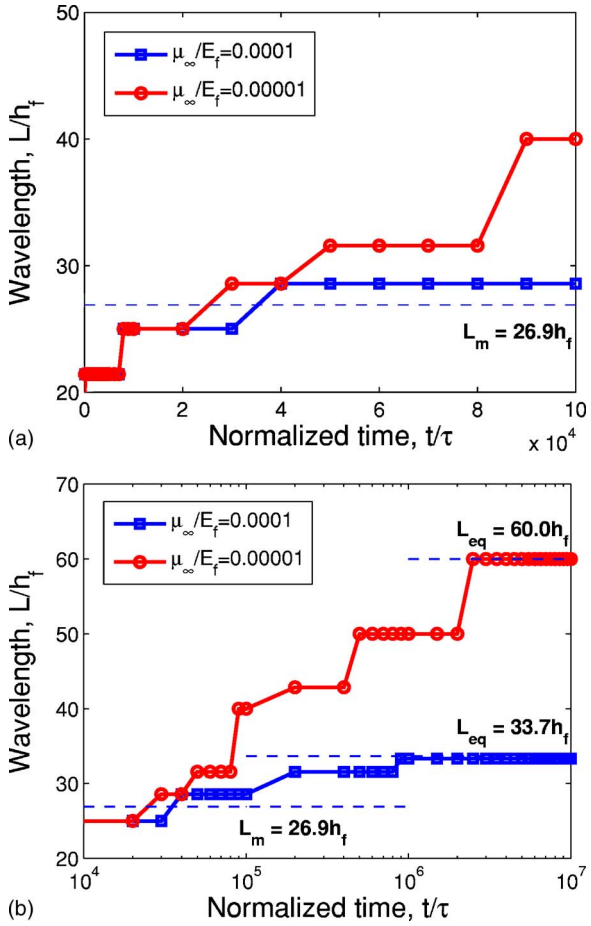

Fig. 6 Evolution of the dominant wrinkle wavelength by numerical simulation: (a) short time evolution and (b) long time evolution

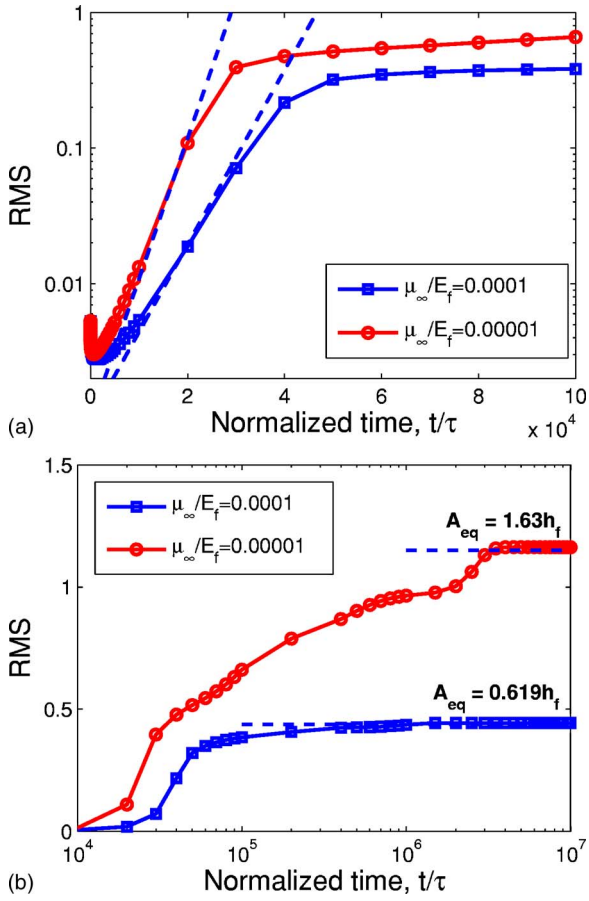

Fig. 7 The root mean square (RMS) of the wrinkle as a function of time: (*a*) short-time evolution and (*b*) long-time evolution

in the numerical simulations, we use $H=10h_f$ as in the metal/polymer bilayer experiments by Yoo and Lee [15]. Figure 3 shows snapshots of the evolving displacements. The amplitude of the lateral deflection grows with time, but the wavelength remains constant for the entire period of the simulation up to $t=50{,}000\tau$. Meanwhile, relatively small in-plane displacement evolves concomitantly, but with a wavelength half of the wrinkle wavelength, as predicted by the equilibrium solution in Eq. (40). Figure 4 shows the wrinkle amplitude as a function of time. The amplitude first grows exponentially, as predicted by the linear perturbation analysis (shown as the straight dashed line). Starting at about $t=20{,}000\tau$, the growth rate deviates from the linear behavior and gradually approaches a plateau. The amplitude essentially remains constant after $t=40{,}000\tau$, indicating that an equilibrium state has been reached. The equilibrium amplitude given by Eq. (38) for the selected wavelength ($L=30h_f$) is $A_{eq}=0.537h_f$, as indicated by the horizontal dotted line in Fig. 4. The result from the numerical simulation agrees closely with the analytical solutions by the linear perturbation analysis at the initial stage and by the energetic analysis for the equilibrium amplitude.

In the above simulation, the wrinkle wavelength is arbitrarily selected *a priori* and the evolution stops when the corresponding equilibrium state is reached. However, the wavelength is not necessarily the equilibrium wavelength selected by energy minimization, as given in Eq. (39). In other words, the equilibrium state reached in the previous simulation is energetically unstable. To further relax the strain energy, continual evolution is possible once the equilibrium state is perturbed with different wavelengths [14]. In real situations, various sources (e.g., thermal fluctuation and surface defects) may induce the initial perturbation, which is random, in general. Figure 5 shows a numerical simulation of evolving wrinkles that starts from a random initial perturbation. The in-plane displacement is again zero initially (not shown). Other parameters are $\sigma_0=-0.01E_f$, $\mu_\infty=0.00001E_f$, $H=10h_f$, $\nu_f=0.3$, and $\nu=0.45$. For each snapshot of the wrinkle, the corresponding Fourier spectrum is shown to the right. Although many wavelengths coexist in the initial perturbation, only those of intermediate wavelengths grow and the fastest growing wavelength dominates at the initial stage. Consequently, an increasingly regular wrinkle emerges from the initially random perturbation. As the evolution continues, the amplitude grows and the wavelength increases. After a sufficiently long time, only one wavelength remains and the wrinkle reaches an equilibrium state. Figure 6 plots the evolution of the dominant wavelength (maximum intensity in the Fourier spectrum), and Fig. 7 shows the root-mean square (rms) of the wrinkle as a function of time. Also plotted in Figs. 6 and 7 are the simulation results with a larger rubbery modulus, $\mu_\infty=0.0001E_f$, for comparison.

From the numerical simulations, three stages of wrinkle evolution can be identified: initial growth of the fastest growing mode, intermediate growth with mode transition, and, finally, an equilibrium wrinkle state. Such behavior qualitatively agrees with the experimental observations in a metal/polymer bilayer film [15]. At the initial stage, the wavelength of the fastest growing mode predicted by the linear perturbation analysis is $L_m=26.9h_f$, which is independent of the rubbery modulus. Figure 6(*a*) shows that the dominant wavelengths in the two simulations are indistinguishable up to $t=2\times10^4\tau$, and the wavelength is close to the predicted value. During this stage, the wrinkle amplitude grows exponen-

tially, but the growth rate depends on the rubbery modulus. In Figure 7(*a*), the two dashed lines indicate the exponential growth predicted by the linear perturbation analysis, where the larger modulus leads to slower growth. At the intermediate stage, both the amplitude and wavelength of the wrinkle evolve toward the equilibrium state. The analytical solutions for the equilibrium state are indicated as dashed lines in Figs. 6(*b*) and 7(*b*). For $\mu_\infty = 0.00001E_f$, the equilibrium wrinkle has a wavelength $L_{eq} = 60.0h_f$ and an amplitude $A_{eq} = 1.63h_f$ (rms$= 1.15h_f$). For $\mu_\infty = 0.0001E_f$, the equilibrium wrinkle has a wavelength $L_{eq} = 33.7h_f$ and an amplitude $A_{eq} = 0.619h_f$ (rms$= 0.438h_f$). The equilibrium states agree closely with the numerical results. It is noted that, although the initial growth is slower, the time to reach the equilibrium state is significantly shorter with the larger rubbery modulus for the viscoelastic layer.

6 Summary

We have developed a nonlinear model for temporal evolution of wrinkles in elastic-viscoelastic bilayer thin films. The model couples a nonlinear theory of elastic plates with a thin-layer approximation of linear viscoelastic responses. Although the model is three-dimensional in nature, the analyses and numerical simulations of the present study have focused on plane-strain deformation. Analytical solutions are obtained for the linear perturbation analysis and the equilibrium state. Numerical simulations illustrate the evolution process from the initial growth to the equilibrium state. The results show that the kinetics of wrinkling strongly depend on the viscoelastic layer.

Acknowledgment

The authors are grateful for the support by NSF Grant No. CMS-0412851 and by the Texas Advanced Technology Program.

References

[1] Iacopi, F., Brongersma, S. H., and Maex, K., 2003, "Compressive Stress Relaxation Through Buckling of a Low-k Polymer-Thin Cap Layer System," Appl. Phys. Lett., **82**, pp. 1380–1382.
[2] Yin, H., Huang, R., Hobart, K. D., Liang, J., Suo, Z., Shieh, S. R., Duffy, T. S., Kub, F. J., and Sturm, J. C., 2003, "Buckling Suppression of SiGe Islands on Compliant Substrates," J. Appl. Phys., **94**, pp. 6875–6888.
[3] Watanabe, M., Shirai, H., and Hirai, T., 2002, "Wrinkled Polypyrrole Electrode for Electroactive Polymer Actuators," J. Appl. Phys., **92**, pp. 4631–4637.
[4] Lacour, S. P., Wagner, S., Huang, Z. Y., and Suo, Z., 2003, "Stretchable Gold Conductors on Elastomeric Substrates," Appl. Phys. Lett., **82**, pp. 2404–2406.
[5] Cerda, E., and Mahadevan, L., 2003, "Geometry and Physics of Wrinkling," Phys. Rev. Lett., **90**, 074302.
[6] Bowden, N., Brittain, S., Evans, A. G., Hutchinson, J. W., and Whitesides, G. M., 1998, "Spontaneous Formation of Ordered Structures in Thin Films of Metals Supported on an Elastomeric Polymer," Nature (London), **393**, pp. 146–149.
[7] Chua, D. B. H., Ng, H. T., and Li, S. F. Y., 2000, "Spontaneous Formation of Complex and Ordered Structures on Oxygen-Plasma-Treated Elastometric Polydimenthylsiloxane," Appl. Phys. Lett., **76**, pp. 721–723.
[8] Martin, S. J., Godschalx, J. P., Mills, M. E., Shaffer II, E. O., and Townsend, P. H., 2000, "Development of a Low-Dielectric-Constant Polymer for the Fabrication of Integrated Circuit Interconnect," Adv. Mater. (Weinheim, Ger.), **12**, pp. 1769–1778.
[9] Stafford, C. M., Harrison, C., Beers, K. L., Karim, A., Amis, E. J., Vanlandingham, M. R., and Kim, H.-C., Volksen, W., Miller, R. D., and Simonyi, E. E., 2004, "A Buckling-Based Metrology for Measuring the Elastic Moduli of Polymeric Thin Films," Nat. Mater., **3**, pp. 545–550.
[10] Groenewold, J., 2001, "Wrinkling of Plates Coupled With Soft Elastic Media," Physica A, **298**, pp. 32–45.
[11] Chen, X., and Hutchinson, J. W., 2004, "Herringbone Buckling Patterns of Compressed Thin Films on Compliant Substrates," J. Appl. Mech., **72**, pp. 597–603.
[12] Huang, Z. Y., Hong, W., and Suo, Z., 2005, "Nonlinear Analysis of Wrinkles in Films on Soft Elastic Substrates," J. Mech. Phys. Solids, **53**, pp. 2101–2118.
[13] Sridhar, N., Srolovitz, D. J., and Suo, Z., 2001, "Kinetics of Buckling of a Compressed Film on a Viscous Substrate," Appl. Phys. Lett., **78**, pp. 2482–2484.
[14] Huang, R., and Suo, Z., 2002, "Wrinkling of an Elastic Film on a Viscous Layer," J. Appl. Phys., **91**, pp. 1135–1142.
[15] Yoo, P. J., and Lee, H. H., 2003, "Evolution of a Stress-Driven Pattern in Thin Bilayer Films: Spinodal Wrinkling," Phys. Rev. Lett., **91**, 154502.
[16] Huang, R., 2005, "Kinetic Wrinkling of an Elastic Film on a Viscoelastic Substrate," J. Mech. Phys. Solids, **53**, pp. 63–89.
[17] Timoshenko, S., and Woinowsky-Krieger, S., 1987, *Theory of Plates and Shells*, 2nd Edition, McGraw-Hill, New York.
[18] Freund, L. B., and Suresh, S., 2003, *Thin Film Materials*, Cambridge University Press, Cambridge.
[19] Christensen, R. M. 1982, *Theory of Viscoelasticity*, Academic Press, New York.
[20] Reynolds, O., 1886, "On the Theory of Lubrication and its Applications to Mr. Beauchamp Tower's Experiments, Including an Experimental Determination of the Viscosity of Olive Oil," Philos. Trans. R. Soc. London, **177**, pp. 157–234.
[21] Xia, Z. C., and Hutchinson, J. W., 2000, "Crack Patterns in Thin Films," J. Mech. Phys. Solids, **48**, pp. 1107–1131.
[22] Huang, R., Prevost, J. H., and Suo, Z., 2002, "Loss of Constraint on Fracture in Thin Film Structures Due to Creep," Acta Mater., **50**, pp. 4137–4148.
[23] Allen, H. G., 1969, *Analysis and Design of Structural Sandwich Panels*, Pergamon, New York.
[24] Huang, Z. Y., Hong, W., and Suo, Z., 2004, "Evolution of Wrinkles in Hard Films on Soft Substrates," Phys. Rev. E, **70**, 030601(R).
[25] Huang, R., and Suo, Z., 2002, "Instability of a Compressed Elastic Film on a Viscous Layer," Int. J. Solids Struct., **39**, pp. 1791–1802.